

Synthesis and evaluation of *N*-(5-fluoro-2-phenoxyphenyl)-*N*-(2-[¹⁸F]fluoromethoxy-*d*₂-5-methoxybenzyl)acetamide: a deuterium-substituted radioligand for peripheral benzodiazepine receptor

Ming-Rong Zhang,^{a,b,*} Jun Maeda,^c Takehito Ito,^{a,b} Takashi Okauchi,^c
Masanao Ogawa,^{a,b} Junko Noguchi,^{a,b} Tetsuya Suhara,^c Christer Halldin^d
and Kazutoshi Suzuki^a

^aDepartment of Medical Imaging, National Institute of Radiological Sciences, 4-9-1 Anagawa, Inage-ku, Chiba 263-8555, Japan

^bSHI Accelerator Service Co. Ltd, 5-9-11 Kitashinagawa, Shinagawa-ku, Tokyo 141-8686, Japan

^cBrain Imaging Project, National Institute of Radiological Sciences, 4-9-1 Anagawa, Inage-ku, Chiba 263-8555, Japan

^dKarolinska Institute, Department of Clinical Neuroscience, Psychiatry Section, Karolinska Hospital, S-17176 Stockholm, Sweden

Received 6 October 2004; revised 24 November 2004; accepted 24 November 2004

Available online 22 December 2004

Abstract—*N*-(5-Fluoro-2-phenoxyphenyl)-*N*-(2-[¹⁸F]fluoromethoxy-*d*₂-5-methoxybenzyl)acetamide ([¹⁸F]**2**) is a potent ligand (IC₅₀: 1.71 nM) for peripheral benzodiazepine receptor (PBR). However, in vivo evaluation on rodents and primates showed that this ligand was unstable and rapidly metabolized to [¹⁸F]F[−] by defluorination of the [¹⁸F]fluoromethyl moiety. In this study, we designed a deuterium-substituted analogue, *N*-(5-fluoro-2-phenoxyphenyl)-*N*-(2-[¹⁸F]fluoromethoxy-*d*₂-5-methoxybenzyl)acetamide ([¹⁸F]**5**) as a radioligand for PBR to reduce the in vivo metabolic rate of the non-deuterated [¹⁸F]**2**. The design principle was based on the hypothesis that the deuterium substitution may reduce the rate of defluorination initiated by cleavage of the C–H bond without altering the binding affinity for PBR. The non-radioactive **5** was prepared by reacting diiodomethane-*d*₂ (CD₂I₂, **6**) with a phenol precursor **7**, followed by treatment with tetrabutylammonium fluoride. The ligand [¹⁸F]**5** was synthesized by the alkylation of **7** with [¹⁸F]fluoromethyl iodide-*d*₂ ([¹⁸F]FCD₂I, [¹⁸F]**9**). Compound **5** displayed a similar in vitro affinity to PBR (IC₅₀: 1.90 nM) with **2**. In vivo evaluation demonstrated that [¹⁸F]**5** was metabolized by defluorination to [¹⁸F]F[−] as a main radioactive component, but its metabolic rate was slower than that of [¹⁸F]**2** in the brain of mice. The deuterium substitution decreased the radioactivity level of [¹⁸F]**5** in the bone of mouse, augmented by the percentage of specific binding to PBR in the rat brain determined by ex vivo autoradiography. However, the PET image of [¹⁸F]**5** for monkey brain showed high radioactivity in the brain and skull, suggesting a possible species difference between rodents and primates.

© 2004 Elsevier Ltd. All rights reserved.

1. Introduction

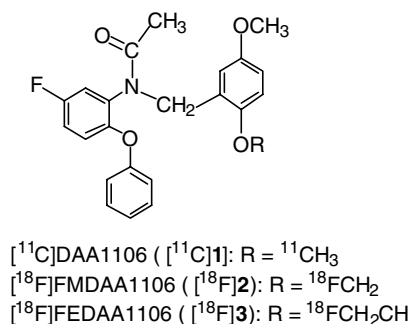
Peripheral benzodiazepine receptor (PBR) is located on the mitochondrial outer membrane in peripheral organs including the kidney, nasal epithelium, lung, heart, and endocrine organs such as the adrenal, testis, and pituitary gland, and in the central nervous system.^{1,2} Since the PBR density was found to increase in injured brains and tumor regions, PBR imaging of PBR in these areas has become an attractive study target.^{3–8} The putative

relationship between PBR and brain diseases (Alzheimer's disease, Parkinson's disease, stroke, encephalitis etc.) or tumors (lung cancer, liver cancer, gastric cancer etc.) has promoted the development of a PET ligand, which could be used for visualizing the distribution and examining the change of PBR in these regions.^{9–12}

We recently developed a PET ligand, [¹¹C]*N*-(2,5-dimethoxybenzyl)-*N*-(5-fluoro-2-phenoxyphenyl)acetamide ([¹¹C]DAA1106, [¹¹C]**1**, Scheme 1), for imaging PBR in the primate brain.^{13,14} The in vitro and in vivo evaluation of mice, rats, and monkeys demonstrated that [¹¹C]**1** had high specific binding with PBR in the brains and had about a 4-fold higher uptake into the monkey brain than [¹¹C]PK 11195,^{15,16} a commonly

Keywords: Peripheral benzodiazepine receptor; Deuterium substitution; Defluorination; PET.

*Corresponding author. Tel.: +81 43 206 4041; fax: +81 43 206 3261; e-mail: zhang@nirs.go.jp



Scheme 1. Chemical structures of $[^{11}\text{C}]\text{DAA1106}$ ($[^{11}\text{C}]\text{1}$) analogues.

used PET ligand for imaging PBR in the primate brain. Now, $[^{11}\text{C}]\text{1}$ is being used to investigate PBR in the human brain in our facility.

Using $[^{11}\text{C}]\text{1}$ as a lead compound, we further synthesized and evaluated two novel $[^{18}\text{F}]\text{alkyl}$ analogues $[^{18}\text{F}]\text{FMDAA1106}$ ($[^{18}\text{F}]\text{2}$) and $[^{18}\text{F}]\text{FEDAA1106}$ ($[^{18}\text{F}]\text{3}$) by replacing the positron emitter ^{11}C for ^{18}F (Scheme 1).^{17,18} The fluoromethyl analogue **2** (IC_{50} : 1.71 nM) and fluoroethyl analogue **3** (0.77 nM) had similar or higher potency for PBR than **1** (1.62 nM). Ligand $[^{18}\text{F}]\text{3}$ had a similar property to $[^{11}\text{C}]\text{1}$ as a potent and specific PET ligand for PBR, and showed 1.5 times higher uptake into the monkey brain than $[^{11}\text{C}]\text{1}$. This promising results led to the clinical investigation of PBR using $[^{18}\text{F}]\text{3}$ to follow $[^{11}\text{C}]\text{1}$. In contrast, although $[^{18}\text{F}]\text{2}$ also passed through BBB and entered into the brain, this ligand exhibited a much higher uptake in monkey skulls, and it had at least 50 times higher radioactivity in the bones of mice than $[^{18}\text{F}]\text{3}$ at 120 min after injection. Metabolite analysis demonstrated that $[^{18}\text{F}]\text{2}$ was rapidly decomposed to $[^{18}\text{F}]\text{F}^-$ in the plasma and brain of mice. The high accumulation of $[^{18}\text{F}]\text{F}^-$ into the bone with a long residence time should decrease the effective signal and give a low sensitivity of PET image of the brain. Moreover, the presence of $[^{18}\text{F}]\text{F}^-$ in the brain could interfere with the determination of 'real' specific binding of $[^{18}\text{F}]\text{2}$ to PBR, and augment non-specific binding in the examined regions.

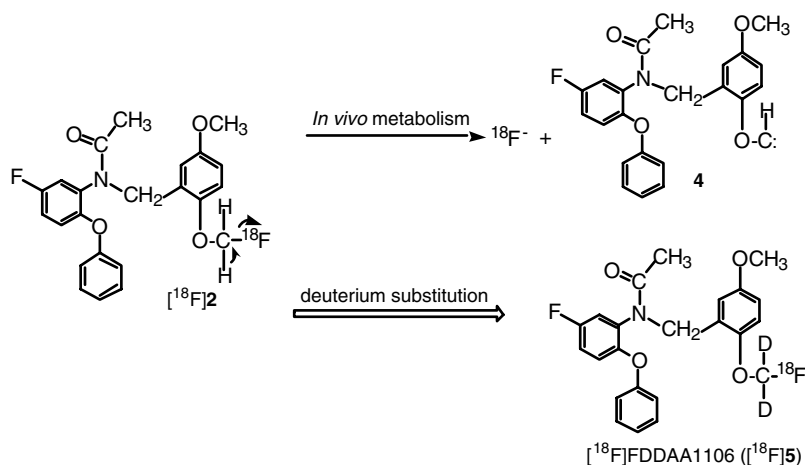
It was demonstrated that defluorination of the fluoromethyl moiety was a main metabolic route of $[^{18}\text{F}]\text{2}$ as shown in Scheme 2.¹⁸ The carbon–hydrogen (C–H) bond of the $[^{18}\text{F}]\text{fluoromethyl}$ moiety may firstly be attacked by enzyme and cleaved, followed by the elimination of hydrofluoride from the same α carbon atom to generate a carbene structure (**4**). Carbene **4** was stabilized by resonating it with the adjacent oxygen atom, which further promoted the decomposition of $[^{18}\text{F}]\text{2}$. Thus, cleavage of the C–H bond is considered as a rate-limiting step, which contributes to the metabolism of $[^{18}\text{F}]\text{2}$.

In this study, we designed a deuterium-substituted analogue of $[^{18}\text{F}]\text{2}$, *N*-(5-fluoro-2-phenoxyphenyl)-*N*-(2- $[^{18}\text{F}]\text{fluoromethoxy-d}_2$ -5-methoxybenzyl)acetamide ($[^{18}\text{F}]\text{5}$), as a novel radioligand for PBR (Scheme 2). The design principle was as follows: since the deuterium atom has a similar and bioisoteric property to the hydrogen atom, deuterium substitution may only have minimal influence on the potential affinity of **5** for PBR. On the other hand, the substitution can be expected to reduce the rate of defluorination of the $[^{18}\text{F}]\text{fluoromethyl}$ moiety since carbon–deuterium (C–D) bond is generally stronger to break than the C–H bond. We firstly synthesized the non-radioactive **5** and its 18-fluorine labeled analogue $[^{18}\text{F}]\text{5}$ and measured the in vitro binding affinity of **5** for PBR. We then compared the metabolic rate of $[^{18}\text{F}]\text{5}$ with that of $[^{18}\text{F}]\text{2}$ in the plasma and brain of mouse, and examined the regional distribution of $[^{18}\text{F}]\text{5}$ in the mice, rats, and monkey.

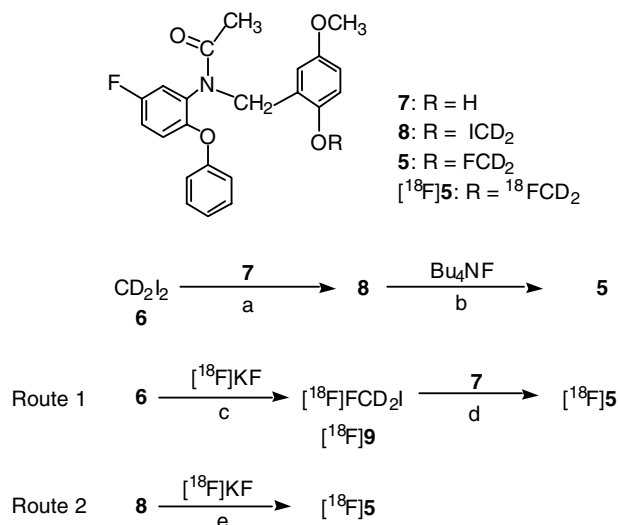
2. Results and discussion

2.1. Chemistry

The non-radioactive fluoromethyl- d_2 analogue **5** was synthesized as shown in Scheme 3. The reaction of excess diiodomethane- d_2 ¹⁷ (CD_2I_2 , **6**) with *N*-(5-fluoro-2-phenoxyphenyl)-*N*-(2-hydroxy-5-methoxybenzyl)acetamide¹⁹ (**7**) in the presence of NaH at 25 °C gave iodomethyl- d_2 analogue **8** and a dimer of **7** as a main



Scheme 2. In vivo metabolism of $[^{18}\text{F}]\text{2}$ and design of $[^{18}\text{F}]\text{5}$.



Scheme 3. Synthesis of **5** and [¹⁸F]**5**: (a) NaH, DMF, 25 °C, 3 h, 15%; (b) THF, reflux, 8 h, 64%; (c) *o*-dichlorobenzene, 110 °C, 2 min, 23%; (d) NaH, DMF, −15 °C, 2 min, 92%; (e) DMF, 30–120 °C, 1–15 min, 0–35%.

by-product. The treatment of **8** with tetrabutylammonium fluoride afforded **5** at a total yield of 10% starting from **7**.

The radiosynthesis of [¹⁸F]**5** was performed by two routes, respectively (Scheme 3). One route was a two-step reaction sequence, which involved the synthesis of the radioactive intermediate [¹⁸F]fluoromethyl-*d*₂ iodide²⁰ ([¹⁸F]FCD₂I, [¹⁸F]**9**), followed by the alkylation of phenol precursor **7** with [¹⁸F]**9**. Another route was the direct nucleophilic replacement of **8** with [¹⁸F]F[−]. In the two-step method, the intermediate [¹⁸F]**9** was prepared by the fluorination of **6** with [¹⁸F]F[−] in the presence of K₂CO₃ and 4,7,13,16,21,24-hexaoxa-1,10-diazabicyclo[8,8,8]hexacosane (Kryptofix 222) as a phase-transfer agent by using an automated synthesis device.²¹ The formed [¹⁸F]**9** was distilled from the reaction mixture, passed through short columns filled with Ascarite and phosphorus pentoxide, and trapped in a DMF solution containing **7** and NaH at −15 °C. This procedure gave a pure and highly reactive [¹⁸F]**9**, since the distillation could leave behind all non-volatile impurities such as metal ions from the cyclotron target, the unreacted [¹⁸F]F[−] and Kryptofix 222/K₂CO₃. After [¹⁸F]**9** trapping was completed, the reaction of **7** with [¹⁸F]**9** proceeded perfectly to form [¹⁸F]**5**. In the direct method, heating **8** with [¹⁸F]F[−] at 30–120 °C could give [¹⁸F]**5**, but the radiochemical yield was not reproducible (0–35%). Moreover, purifying the product from the reaction mixture was often complicated because excess Kryptofix/K₂CO₃ and the impurities resulting from the target significantly decreased the purification efficiency. Thus, [¹⁸F]**5** was synthesized by the two-step reaction method via [¹⁸F]**9** for animal experiments.

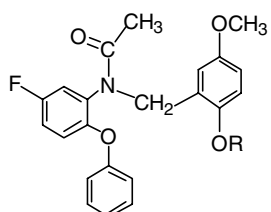
Semi-preparative HPLC purification on the reverse phase for the reaction mixture gave [¹⁸F]**5** in 13 ± 6% (*n* = 4) radiochemical yield based on [¹⁸F]F[−], corrected for the decay at the end of bombardment in a syn-

thesis time of 50 ± 3 min. The identity of the desired product was confirmed by co-injection with the non-radioactive **5** using analytic HPLC. In the final product solution, the radiochemical purity of [¹⁸F]**5** was higher than 98% with a specific activity of 40–70 GBq/μmol as determined from the mass measured by the HPLC/UV analysis. No significant peak corresponding to **7** or other impurities relative to **7** was observed in the HPLC chart for the final product. Moreover, the radiochemical purity of [¹⁸F]**5** remained >95% after it was left at 25 °C for 180 min, and this product was stable as a PET ligand while performing animal experiments.

2.2. Evaluation

In a previous study, the rapid metabolism of fluoromethyl ligand [¹⁸F]**2** by defluorination in the brain and plasma precluded its usefulness for the clinical investigation of PBR.¹⁸ The high accumulation of [¹⁸F]F[−] in the bone including the skull with a long residence time could decrease the effective signal of PET imaging of [¹⁸F]**2** in the brain and create difficulties on the data analysis. Furthermore, the presence of [¹⁸F]F[−] might augment the non-specific binding in the examined regions, and then interfere with the determination of the specific binding for PBR. It was found that [¹⁸F]F[−] was generated by *in vivo* defluorination, which might be initiated by cleavage of the C–H bond as a rate-limiting step. Therefore, to reduce the rate of defluorination starting from break of the C–H bond, we considered the usefulness of the isotopic effect of deuterium on hydrogen. Due to the lower zero-point energy (difference: 6–9 kJ/mol) and the lower vibration frequency (difference: 788 cm^{−1}) of the C–D bond than the C–H bond, the C–D bond is generally more difficult to break than the C–H bond.²² It was reported that the cleaving rate of the C–H bond was about 6.7 times faster at 25 °C, and 3.3 times faster at 200 °C than that of C–D.²² There were several examples of the deuterium-substituted PET ligands for MAO B²³ and 5-HT_{2A}²⁴ receptors improving the properties of the corresponding non-deuterated ligands by reducing their *in vivo* metabolic rates. In this study, we compared the *in vitro* binding affinity, metabolic rate and regional distribution of [¹⁸F]**5** with those of the non-deuterated [¹⁸F]**2**.

2.2.1. In vitro binding affinity for PBR and CBR. The *in vitro* binding affinities (IC₅₀) of **5** and **8** for PBR were measured from competition for the [¹¹C]**1** binding using quantitative autoradiography according to the procedures as described previously.^{18,25} As shown in Table 1, **5** displayed a similar affinity than **2** for PBR, and this value was also little lower than that of **1** and about 4-fold higher than PK 11195. The iodomethyl-*d*₂ analogue **8** had about 27 times weaker affinity than **5**, suggesting that the relative bulk group contained in this series of derivatives was not favorable for expressing the binding potency of PBR. On the other hand, **5** and **8** displayed negligible affinities for central benzodiazepine receptor (CBR) measured by using CBR-selective [¹¹C]flumazenil. The high selectivity of PBR/CBR of the two analogues may be due to their structural difference from the typical benzodiazepine structure.²⁰ Although the

Table 1. In vitro binding affinity (IC_{50}) for PER and CBR, and octanol/phosphate buffer distribution coefficient ($\log P$)


Ligand	R	$IC_{50}(nM)^a$		$\log P^d$
		PBR ^b	CBR ^c	
5	FCD2	1.90	>10,000	3.76
8	ICD2	52.30	>10,000	4.26
2	FCH2	1.71	>10,000	3.70
1	CHS	1.62	>10,000	3.65
PK11195		8.26	>10,000	

^a Values represent the mean obtained from nine concentrations of compound using at least eight slices of rat brain ($n = 3$).

^b [3H]DAA1106 was incubated in the presence of the compounds examined.

^c [3H]Flumazenil was incubated in the presence of the compounds examined.

^d The $\log P$ values were determined in the phosphate buffer (pH = 7.4)/octanol system using the shaking flask method. All results were presented as mean values ($n = 3$) with a maximum range of $\pm 5\%$.

deuterium atom is larger than hydrogen, the deuterium substitution does not alter the molecular similarity and bioisoteric property between the two functional groups of $O-CD_2F$ and $O-CH_2F$. The difference between the two molecules is too small to have significant influence on their affinities for PBR.

2.2.2. Metabolism in the plasma and brain of mouse. The metabolite analysis of [^{18}F]5 was performed in the brain and plasma of mice. After i.v. injection of [^{18}F]5 (8 MBq) into mice ($n = 3$) at designated time points, the plasma and brain homogenate were obtained and immediately deproteinized with CH_3CN . Extraction of the radioactivity in the plasma and brain homogenate into CH_3CN was efficient, and the recovered yield was >70%. The radioactive metabolite of [^{18}F]5 was identified using HPLC with a highly sensitive detector²⁶ for radioactivity. In all samples, a radioactive component was determined in addition to the unchanged [^{18}F]5. As estimated by its retention time ($t_R = 2.0$ min), this metabolite was much more polar than [^{18}F]5 ($t_R = 10.2$ min). Moreover, the t_R of the peak remained unchanged when treated with a base or acid. Using ion exchange chromatography and TLC, this product was assigned to [^{18}F]F[−], which was identified by co-injecting and developing with non-radioactive standard KF solution. As it was improbable brain permeable, [^{18}F]F[−] was produced in the plasma and brain, respectively. This result suggested that defluorination of the [^{18}F]fluoromethyl moiety was the main metabolic route of [^{18}F]5, and the deuterium substitution did not change its main metabolism route.

Figure 1 shows the percentages of unchanged [^{18}F]5 and [^{18}F]2 in the plasma and brain of mice measured by

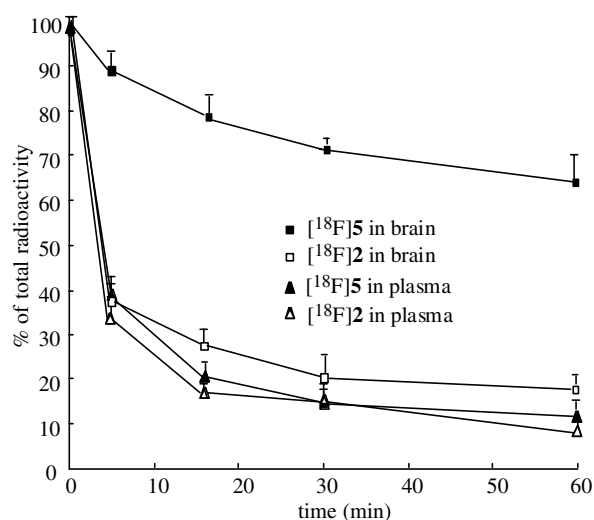


Figure 1. Percentage (mean \pm s.d., $n = 3$) conversion of [^{18}F]5 to metabolite in the mouse plasma and brain at several time points after i.v. injection of [^{18}F]5 (5–10 MBq) into the mice. The unchanged [^{18}F]5 and metabolite were analyzed by HPLC for CH_3CN extracts from the plasma and brain homogenate prepared as described in the experimental.

HPLC. We conducted two-way repeated ANOVA to compare the time courses of [^{18}F]5 with those of [^{18}F]2 in the brain and plasma, respectively. In the plasma, no significant interaction was determined between the two ligands. The half life ($T_{1/2}$) in the plasma was 2.575 min for [^{18}F]5 and 2.367 min for [^{18}F]2. In the brain, a significant interaction ($F_{1/16} = 83.93$, $P < 0.01$) was determined between them. The half life ($T_{1/2}$) of [^{18}F]5 in the brain was >60 min, whereas that of [^{18}F]2 was only 2.227 min. The mechanism of the different metabolic rates between the two ligands in the brain was that the C–D bond of [^{18}F]5 was more difficult to break by enzyme than the C–H bond of [^{18}F]2, which was the rate-limiting step contributory to their metabolism.

The difference of the metabolic rates of [^{18}F]2 and [^{18}F]5 in mouse brain was remarkable, compared with that in the mouse plasma. We considered that a same enzyme is related to their metabolism in the plasma and brain. In general, the level of enzyme metabolizing a parent ligand in plasma is much higher than that in brain. Therefore, the different level of the same enzyme metabolizing [^{18}F]2 and [^{18}F]5 in the brain and plasma was a contributing factor for the difference of their metabolic rates. The level of enzyme attacking the C–H and C–D bonds in the plasma may be too high to distinguish difference of the two bonds, whereas that in the brain may be apt to realize the difference.

2.2.3. Regional distribution. The radioactivity distribution of [^{18}F]5 in the mice was examined and compared to that of [^{18}F]2 at 5–120 min after injection. Table 2 shows the decay-corrected percent dose per gram (% ID/g) data of [^{18}F]2 and [^{18}F]5 in the brain, blood and bone. The radioactivity level of [^{18}F]5 in the bone was 1.6% ID/g at 120 min after injection, and was 30% of [^{18}F]2 level in the bone. On consideration of the ten-

Table 2. Distribution (% injected dose/g tissue: mean \pm s.d., $n = 3$) of [^{18}F]ligand in Mice at 5, 15, 30, 60, and 120 min after injection

Ligand	Tissue	5 min	15 min	30 min	60 min	120 min
[^{18}F]2	Blood	0.95 \pm 0.09	1.34 \pm 0.54	0.76 \pm 0.32	0.54 \pm 0.18	0.49 \pm 0.18
	Brain	2.65 \pm 0.85	3.26 \pm 1.07	4.39 \pm 1.38	4.04 \pm 1.95	3.47 \pm 0.94
	Bone	0.58 \pm 0.23	1.98 \pm 1.99	2.51 \pm 1.35	3.91 \pm 0.86	5.64 \pm 0.72
[^{18}F]5	Blood	0.78 \pm 0.23	0.92 \pm 0.15	0.83 \pm 0.20	0.86 \pm 0.33	0.52 \pm 0.15
	Brain	2.31 \pm 0.92	2.93 \pm 1.01	3.68 \pm 1.43	3.62 \pm 0.85	3.24 \pm 0.70
	Bone	0.58 \pm 0.29	0.74 \pm 0.05	1.23 \pm 0.08	1.59 \pm 0.01	1.63 \pm 0.04

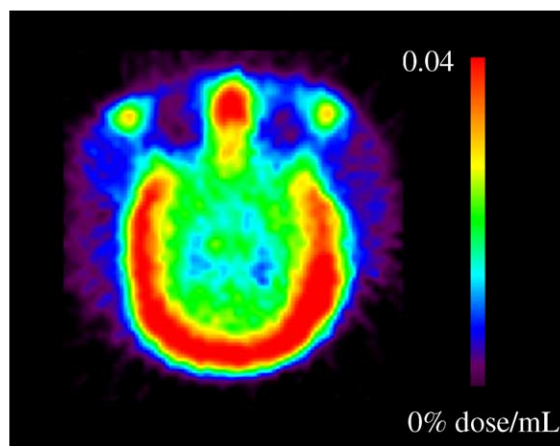
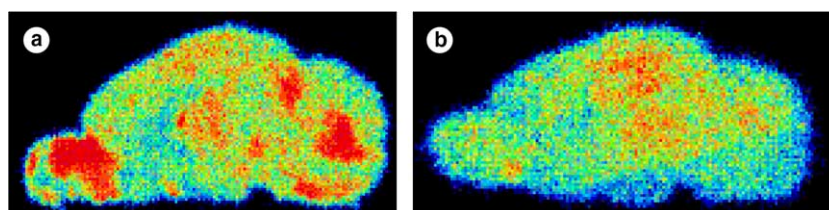
dency of [^{18}F]F $^-$ to readily accumulate in bone, the radioactivity examined in the bone was mostly due to [^{18}F]F $^-$. In contrast, [^{18}F]2 and [^{18}F]5 displayed a similar level of radioactivity in the brain and blood. The cause may be that the two ligands had similar affinity for PBR, lipophilicity and other physiochemical properties. Although they were metabolized in the brain in different rates after they entered into the brain, the main radioactive metabolite [^{18}F]F $^-$ may be retained in the brain without a rapid clearance, which did not give significant difference for their total radioactivity levels in the brain.

Figure 2 shows ex vivo autoradiograms of rat brains at 30 min after injection of [^{18}F]5. As can be seen in the sagittal section of the control brain (Fig. 2a), [^{18}F]5 showed a high uptake, consistent with the distribution data measured above (Table 2). High radioactivity levels were observed in the olfactory bulb and cerebellum, whereas low uptakes were seen in the other brain regions such as the frontal cortex and striatum. The uptake pattern of radioactivity was in accordance with the regional distribution of PBR in the brain and was similar to those of [^{11}C]1 and [^{18}F]3.^{14,17,27} Co-injection of [^{18}F]5 with the non-radioactive **1** (1 mg/kg) produced a reduction of radioactivity in the brain regions having PBR (Fig. 2b). The radioactivity level in the olfactory bulb and cerebellum was decreased to 30–40% of the control, while the reduction ratio of [^{18}F]2 by **1** was about 50%.¹⁸ In spite of remarkable difference of the metabolic rate of the two ligands in the brain, the difference of their non-specific bindings determined by ex vivo autoradiography was not so significant. From the metabolic route of [^{18}F]2 and [^{18}F]5, we considered that the nonspecific binding of the two ligands was mainly due to [^{18}F]F $^-$ in the brain. Although [^{18}F]F $^-$ does not bind to the receptor, the [^{18}F]F $^-$ might be partly retained in the olfactory bulb and cerebellum, and could not be released by the co-injection of **1**, which kept the nonspecific binding of [^{18}F]2 and [^{18}F]5 at a similar level. The left [^{18}F]F $^-$ might spread around the brain and did not clear out

from the brain rapidly, which led to a different distribution of [^{18}F]F $^-$ in the whole brain. In fact, the ratio of olfactory bulb to frontal cortex was 2.1 ± 0.3 for [^{18}F]5, whereas the ratio for [^{18}F]2 was only 1.6 ± 0.5 in the corresponding regions. This finding supported that the [^{18}F]F $^-$ level was lower for [^{18}F]5 than for [^{18}F]2 in the whole brain including the frontal cortex.

Figure 3 shows a typical PET summation image of monkey brain acquired from 30 to 180 min after [^{18}F]5 injection (80 MBq/1.5 mL). Unexpectedly, although a high radioactivity was observed in the monkey brain, the PET image of [^{18}F]5 displayed much higher accumulation of radioactivity in skull. Moreover, the level of radioactivity of [^{18}F]5 in the monkey skull was similar to that of [^{18}F]2¹⁸ by comparing their PET images at a normalized injection dose. This image gave a visual evidence that [^{18}F]5 was metabolized by in vivo defluorination to [^{18}F]F $^-$, which was accumulated into the bone.

In this study, the isotopic effect induced a distinct reduction in the metabolic rate of [^{18}F]5 in the brain of mice

**Figure 3.** PET summation image of the monkey brain acquired between 30 and 180 min after [^{18}F]5 injection (80 MBq).**Figure 2.** Ex vivo autoradiogram of [^{18}F]5 in the sagittal sections of rat brains at 30 min after injection (20–25 MBq). (a) [^{18}F]5; (b) [^{18}F]5+**1** (1 mg/kg).

although the deuterium substitution did not change the main metabolism profile of [^{18}F]5. The decreased rate of [^{18}F]5 reduced the uptake of [^{18}F]F $^-$ in the bone of mice, and increased slightly the percentage of specific binding to PBR accounting for the total binding as reflected in the autoradiogram of the rat brain. However, the PET image of [^{18}F]5 for the monkey brain was not improved in comparison with [^{18}F]2, which was disturbed by [^{18}F]F $^-$ accumulating into the skull. The significant difference of radioactivity distribution in the bones of mice or rats and monkeys may reflect the species difference between rodents and primates. Therefore, unlike [^{11}C]1 and [^{18}F]3, [^{18}F]5 may be not a useful PET radioligand, even though it entered the brain and had some specific binding with PBR in the brain. The high accumulation of [^{18}F]F $^-$ in the bone should preclude the in vivo usefulness of [^{18}F]5 for determining PBR binding in the primate brain. Moreover, the uptake of [^{18}F]F $^-$ should decrease the effective signal of PET image and the accuracy of data if this ligand was employed to quantitatively measure the PBR density in the brain.

3. Conclusion

In this study, the deuterium-substituted [^{18}F]5 for PBR was designed, synthesized, and evaluated. Ligand [^{18}F]5 was synthesized by the alkylation of the desmethyl precursor 7 with [^{18}F]9 in reproducible radiochemical yields. Compared with the non-deuterated [^{18}F]2, [^{18}F]5 displayed a slower metabolic rate in the brain of mice, a lower uptake into the mouse bone, and higher specific binding to PBR in the rat brain with a similar binding affinity for PBR. However, the deuterium substitution did not decrease the radioactivity level of [^{18}F]5 in the monkey skull due to its remarkable in vivo defluorination, suggesting species difference between rodents and primates. Although [^{18}F]5 was not be used for the in vivo investigation of PBR in the primates, our results indicated that isotope effect is an effective tool for improving in vivo behaviors of a parent radioligand.

4. Experimental

4.1. General

^1H NMR spectra were recorded on a JNM-GX-270 spectrometer (JEOL, Tokyo) with tetramethylsilane as an internal standard. All chemical shifts (δ) were reported in parts per million (ppm) downfield from the standard. FAB-MS were obtained on a JEOL NMS-SX102 spectrometer (JEOL, Tokyo). Column chromatography was performed on Merck Kieselgel gel 60 F $_{254}$ (70–230 mesh). 18-Fluorine (^{18}F) was produced by $^{18}\text{O}(\text{p},\text{n})^{18}\text{F}$ nuclear reaction using a CYPRIS HM-18 cyclotron (Sumitomo Heavy Industry, Tokyo). If not otherwise stated, radioactivity was measured with an IGC-3R Curiometer (Aloka, Tokyo). HPLC was performed using a JASCO HPLC system (JASCO, Tokyo): effluent radioactivity was monitored using a NaI (TI) scintillation detector system. All chemical reagents with the highest grade commercially available were pur-

chased from Aldrich Chem. (Milwaukee) and Wako Pure Chem. Ind. (Osaka). The animal experiments were performed according to the recommendations of the committee for the care and use of laboratory animals, National Institute of Radiological Sciences (NIRS).

4.2. Chemical synthesis

4.2.1. *N*-(5-Fluoro-2-phenoxyphenyl)-*N*-(2-iodomethoxy-*d* $_2$ -5-methoxybenzyl)acetamide (8). A mixture of *N*-(5-fluoro-2-phenoxyphenyl)-*N*-(2-hydroxy-5-methoxybenzyl)acetamide 19 (7, 38 mg, 0.10 mmol), CD $_2$ I $_2$ (6, 32 μL , 0.40 mmol), and NaH (8 mg, 0.34 mmol) in DMF (2 mL) was stirred at 25 $^\circ\text{C}$ for 3 h. The reaction was stopped with AcOEt, and rinsed with water and saturated NaCl solution. After the organic layer was dried over Na $_2$ SO $_4$, the solvent was removed to give a residue. Column chromatograph of the residue on silica gel with CHCl $_3$ /hexane (1/20) gave 8 (8.0 mg, 15%) as a colorless oil; ^1H NMR (300 MHz, CDCl $_3$) δ : 7.18–7.40 (2H, m), 6.15–7.33 (9H, m), 4.71 (dd, J = 7, 46 Hz), 3.78 (3H, s), 2.20 (3H, s); FABMS (m/z): 524.1 (M^+ +1); Anal. (C $_{23}\text{H}_{19}\text{D}_2\text{FINO}_4$) C, H, N.

4.2.2. *N*-(5-Fluoro-2-phenoxyphenyl)-*N*-(2-fluoromethoxy-*d* $_2$ -5-methoxybenzyl)acetamide (5). A mixture of 8 (16 mg, 0.03 mmol) and tetrabutylammonium fluoride (1.0 M solution in THF, 2.0 mL) was heated at reflux for 8 h. After THF was removed, the reaction mixture was re-dissolved in AcOEt, and rinsed with water and saturated NaCl solution. After the organic layer was dried over Na $_2$ SO $_4$, the solvent was removed to give a residue. Column chromatograph of the residue on silica gel with CHCl $_3$ /hexane (1/20) gave 5 (10 mg, 70%) as a colorless oil; ^1H NMR (300 MHz, CDCl $_3$) δ : 7.38–7.49 (2H, m), 6.71–7.13 (8H, m), 6.28–6.44 (1H, m), 4.75 (2H, dd, J = 7, 46 Hz), 3.71 (3H, s), 2.12 (3H, s); FABMS (m/z): 416.3 (M^+ +1); Anal. (C $_{23}\text{H}_{19}\text{D}_2\text{F}_2\text{NO}_4$) C, H, N.

4.3. Radiosynthesis

4.3.1. [^{18}F]Fluoride ([^{18}F]F $^-$). [^{18}F]F $^-$ was produced by the $^{18}\text{O}(\text{p},\text{n})^{18}\text{F}$ reaction on 10–20 atom% H $_2$ ^{18}O using 18 MeV protons (14.2 MeV on target) from the cyclotron and separated from [^{18}O]H $_2\text{O}$ using Dowex 1-X8 anion exchange resin in an irradiating room. The produced [^{18}F]F $^-$ was released from the resin with aqueous K $_2$ CO $_3$ (3.3 mg/0.3 mL) into a vial containing CH $_3$ CN (1.5 mL)/Kryptofix 222 (25 mg) and transferred into a reaction vessel set in a hot cell.

4.3.2. *N*-(5-Fluoro-2-phenoxyphenyl)-*N*-(2-[^{18}F]fluoromethoxy-*d* $_2$ -5-methoxybenzyl)acetamide ([^{18}F]5). After [^{18}F]F $^-$ in the reaction vessel was dried to remove H $_2\text{O}$ and CH $_3$ CN at 120 $^\circ\text{C}$ for 20 min, 6 (200 μL) in *o*-dichlorobenzene (200 μL) was added into the radioactive mixture. Under a He flow (50 mL/min), the resulted [^{18}F]FCD $_2$ I ([^{18}F]9) was immediately distilled at 110 $^\circ\text{C}$ for 2 min and bubbled in another reactor containing 7 (1.5 mg) and NaH (10 μL , 1.5 g/20 mL DMF) in anhydrous DMF (300 μL) at -15 $^\circ\text{C}$. After maximum radioactivity was trapped into the solution, the reaction was

terminated by adding CH₃CN/H₂O (6/4, 500 μ L) and the reaction mixture was applied to a semi-preparative HPLC system. HPLC purification was performed on YMC J'sphere ODS-H80 column (10 mm ID \times 250 mm) using a mobile phase of CH₃CN/H₂O (60/40) at a flow rate of 6.0 mL/min. The retention time (t_R) for [¹⁸F]**5** was 12.8 min, while that for **7** was 6.7 min. The radioactive fraction corresponding to [¹⁸F]**5** was collected in a sterile flask containing polysorbate (80) (75 μ L) and ethanol (150 μ L), evaporated to dryness under vacuum, redissolved in sterile normal saline (7 mL) and passed through a 0.22 μ m Millipore filter to obtain the final product. At the end of synthesis, 100–180 MBq ($n = 4$) of [¹⁸F]**5** was obtained as an i.v. injectable solution at a beam current of 10–15 μ A and 20–25 min proton bombardment.

4.4. Radiochemical purity and specific activity determinations

Radiochemical purity was assayed by analytical HPLC (column: CAPCELL PAK C₁₈, 4.6 mm ID \times 250 mm, UV at 254 nm; mobile phase: CH₃CN/H₂O = 6/4). The t_R for [¹⁸F]**5** was 6.1 min at a flow rate of 2.0 mL/min. The specific activity of [¹⁸F]**5** was calculated by comparing the assayed radioactivity (GBq) with the mass measured from a calibration curve obtained by the carrier UV peaks at 254 nm corresponding to five known concentrations.

4.5. In vitro binding assays

Male Sprague–Dawley rats ($n = 3$) weighing 220–250 g were sacrificed by decapitation under ether anesthesia, and their brains were quickly removed and frozen on powdered dry ice. Brain sagittal sections (20 μ m) were cut on a cryostat microtome (HM560, Leica, Bensheim) and thaw-mounted on glass slides (Matsunami Glass Ind., Tokyo), which were then dried at 25 °C and stored at –18 °C until used for experiments. The brain sections were pre-incubated at 25 °C for 20 min in 50 mM Tris–HCl (pH 7.4) buffer. After pre-incubation, these sections were incubated at 37 °C for 30 min in assay buffer containing [¹¹C]**1** (about 1 nM, specific activity: 100 GBq/ μ mol) or [¹¹C]flumazenil (about 1 nM, specific activity: 190 GBq/ μ mol). To determine the IC₅₀ values of **5** and **8** for the [¹¹C]**1** (for PBR) or [¹¹C]flumazenil (for CBR) binding, the brain sections were incubated with [¹¹C]**1** or [¹¹C]flumazenil using **5** and **8** at nine different concentrations (0.1–1000 nM), respectively. Ten micrometers of **1** or flumazenil was used to determine the nonspecific binding for PBR or CBR in the brains. After incubation, the brain sections were washed three times for 2 min each time with cold assay buffer, dipped into cold distilled water for 10 s, and dried with a warm air flow (about 50 °C). These sections were then placed in contact with imaging plates (BAS-SR 127, Fuji Photo Film, Tokyo) for 60 min to analyze their radioactivity distribution with a FUJIX BAS 1800 bioimaging analyzer (Fuji). Region of interest (ROI) in the sections was identified in the cerebellum. PSL data corresponding to radioactivity in the cerebellum in the presence and absence of the displacement **5** and **8** were deter-

mined, respectively. The specific binding for PBR or CBR was defined as total binding minus nonspecific binding of [¹¹C]**1** or [¹¹C]flumazenil. PSL data corresponding to specific binding at each compound concentration were calculated as a percentage in relation to the control specific binding, and were converted to probit values to determine the IC₅₀ of each compound.

4.6. Metabolite analysis for mouse plasma and brain tissue

After i.v. injection of [¹⁸F]**5** or [¹⁸F]**2** (5–10 MBq/100 μ L) into ddy mice ($n = 3$), these mice were sacrificed by cervical dislocation at 5, 15, 30, 60 or 120 min. Blood (0.7–1.0 mL) and whole brain samples were removed quickly, respectively. The blood sample was centrifuged at 15,000 rpm (3615 Model, Kubota, Tokyo) for 2 min at 4 °C to separate plasma, which (250 μ L) was collected in a test tube containing CH₃CN (500 μ L) and **5** or **2** (10 μ L, 1.5 mg/5.0 mL of CH₃CN). After the tube was vortexed for 15 s and centrifuged at 15,000 rpm for 2 min for deproteinization, the supernatant was collected. The extraction efficiency of radioactivity into the CH₃CN supernatant ranged from 70–92% of the total radioactivity in the plasma. On the other hand, the cerebellum and forebrain including the olfactory bulb were dissected from the mouse brain and homogenized together in an ice-cooled CH₃CN/H₂O (1/1, 1.0 mL) solution. The homogenate was centrifuged at 15,000 rpm for 2 min at 4 °C and the supernatant was collected. The recovery percentage of radioactivity into the supernatant was 74–90% of the total radioactivity in the brain homogenate.

An aliquot of the supernatant (100–500 μ L) obtained from the plasma or brain homogenate was injected into the HPLC with a highly sensitive detector²⁵ for radioactivity, and analyzed under the same HPLC conditions described above except the mobile phase of CH₃CN/H₂O with a ratio of 1/1. The percent ratio of [¹⁸F]ligand to the total radioactivity (corrected for decay) on the HPLC chromatogram was calculated as % = (peak area for [¹⁸F]ligand/total radioactive peak area) \times 100.

4.7. Biodistribution in mice

A saline solution of [¹⁸F]**5** or [¹⁸F]**2** (average of 8 MBq/200 μ L, specific activity: 55 GBq/ μ mol) was injected into ddy mice (30–40 g, 9 weeks, male; $n = 3$) through the tail vein. Three mice for each time point were sacrificed by cervical dislocation at 5, 15, 30, 60, and 120 min after injection, respectively. The whole brain, bone and blood samples were quickly removed and weighed. The radioactivity present in the various tissues were measured in a Packard autogamma scintillation counter, and expressed as a percentage of the injected dose per gram of wet tissue (% ID/g). All radioactivity measurements were corrected for decay.

4.8. Ex vivo autoradiography

A saline solution of [¹⁸F]**5** (20 MBq/200 μ L, specific activity: 65 GBq/ μ mol) or a mixture of [¹⁸F]**5**

(25 MBq/200 μ L) and **1** (1 mg/kg, 200 μ L) was injected into a male Sprague–Dawley rat (220–250 g, 9 weeks, male) through the tail vein. At 30 min after injection, the rat was sacrificed by decapitation under ether anesthesia, and the brain was quickly removed and frozen on powdered dry ice. Brain sagittal sections (20 μ m) were cut on a cryostat microtome (HM560) and thaw-mounted on glass slides (Matsunami Glass Ind., Tokyo), dried with warm air flow (about 50 °C). These sections were then placed in contact with imaging plates (BAS-SR 127) for 60 min to analyze the radioactivity distribution with the FUJIX BAS bioimaging analyzer (Fuji).

4.9. Monkey PET

PET scan was performed using a high-resolution SHR-7700 PET camera (Hamamatsu Photonics, Hamamatsu) designed for laboratory animals, which provides 31 transaxial slices 3.6 mm (center-to-center) apart and a 33.1 cm field of view. A male rhesus monkey (*Macaca mulatta*) weighing about 5 kg was repeatedly anesthetized with ketamine (Ketalar[®], 10 mg/kg/h, i.m.) every hour throughout the session. After a transmission scan for attenuation correction for 1 h using 74 MBq ⁶⁸Ge–⁶⁸Ga source, a dynamic emission scan in 3D acquisition mode was performed for 180 min (2 min \times 5 scans, 4 min \times 10 scans, 10 min \times 4 scans). All emission scan images were obtained by treatment using an image analysis software.^{28,29} A saline of [¹⁸F]**5** (80 MBq) was injected i.v. into the monkey, and time-sequential tomographic scanning was performed on a transverse section of the brain for 180 min.

Acknowledgements

The authors are grateful to Taisho Pharmaceutical Co., Ltd for giving us the samples (DAA1106: **1** and precursor: **7**) and helpful suggestions. We also thank the staff of the Cyclotron Operation Section, Radiopharmaceutical Chemistry Section and Brain Imaging Project of National Institute of Radiological Sciences (NIRS) for their support in the operation cyclotron operation, radioisotope production and PET experiment.

References and notes

- Braestrop, C.; Squires, R. F. *Proc. Natl. Acad. Sci. U.S.A.* **1977**, *74*, 1839.
- Papadopoulos, V.; Amri, H.; Li, H.; Yao, Z.; Brown, R. C.; Vidic, B.; Culty, M. Structure, function and regulation of the mitochondrial peripheral-type benzodiazepine receptor. *J. Pharmacol. Exp. Ther.* **2001**, *299*, 793–800.
- Diorio, D.; Welner, S.; Butterworth, R.; Meaney, M.; Suranyl-Cadotte, R. *Neurobiol. Aging* **1991**, *12*, 255.
- Banati, R. B.; Newcombe, J.; Gunn, R. N.; Cagnin, A.; Turkheimer, F.; Heppner, F.; Price, G.; Wegner, F.; Giovannoni, G.; Miller, D. H.; Perkin, G. D.; Smith, T.; Hewson, A. K.; Bydder, G.; Kreutzberg, G. W.; Jones, T.; Cuzner, M. L.; Myers, R. *Brain* **2000**, *123*, 2321.
- Raghavendra Rao, V. L.; Dogan, A.; Bowen, K. K.; Dempsey, R. J. *Exp. Neurol.* **2000**, *161*, 102.
- Batra, S.; Iosif, C. S. *Int. J. Oncol.* **1998**, *12*, 1295.
- Miyazawa, N.; Hamel, E.; Diksic, M. *J. Neurooncol.* **1998**, *38*, 19.
- Venturini, I.; Zeneroli, M. I.; Corsi, L.; Avallone, R.; Farina, F.; Alho, H.; Baraldi, C.; Ferrarese, C.; Pecora, N.; Frigo, M.; Ardizzone, G.; Arrigio, A.; Pellicci, R.; Baraldi, M. *Life Sci.* **1998**, *63*, 1269.
- Camsonne, R.; Crouzel, C.; Comar, D.; Maziere, M.; Prenant, C.; Sastre, J.; Moulin, M. A.; Syrota, A. *J. Labelled Comp. Radiopharm.* **1984**, *21*, 985.
- Pike, V. W.; Halldin, C.; Crouzel, C.; Barre, L.; Nutt, D. J.; Osman, S.; Shah, F.; Turton, D. R.; Waters, S. L. *Nucl. Med. Biol.* **1993**, *20*, 503.
- Cappelli, A.; Anzini, M.; Vomero, S.; De Benedetti, P. G.; Menziani, M. C.; Giorgi, G.; Manzoni, C. *J. Med. Chem.* **1997**, *40*, 2910.
- Matarrese, M.; Moresco, R. M.; Cappelli, A.; Anzini, M.; Vomero, S.; Simonelli, P.; Verza, E.; Magni, F.; Sudati, F.; Soloviev, D.; Todde, S.; Carpinelli, A.; Kienle, M. G.; Fazio, F. *J. Med. Chem.* **2001**, *44*, 579.
- Zhang, M.-R.; Kida, T.; Noguchi, J.; Furutsuka, K.; Maeda, J.; Suhara, T.; Suzuki, K. *Nucl. Med. Biol.* **2003**, *30*, 513.
- Maeda, J.; Suhara, T.; Zhang, M.-R.; Okauchi, T.; Ichimiya, T.; Inajii, M.; Ohbayashi, S.; Suzuki, K. *Synapse* **2004**, *52*, 283.
- Pappata, P.; Cornu, Y.; Samson, C.; Prenant, J.; Benavides, B.; Scatton, C.; Crouzel, J. J.; Hauw, A.; Syrota, A. *J. Nucl. Med.* **1991**, *32*, 1608.
- Cagnin, A.; Brooks, D. J.; Kennedy, A. M.; Gunn, R. N.; Myers, R.; Turkheimer, F. E.; Jones, T.; Banati, R. B. *Lancet* **2001**, *358*, 461.
- Zhang, M.-R.; Maeda, J.; Furutsuka, K.; Yoshida, Y.; Ogawa, M.; Suhara, T.; Suzuki, K. *Bioorg. Med. Chem. Lett.* **2003**, *13*, 201.
- Zhang, M.-R.; Maeda, J.; Ogawa, M.; Noguchi, J.; Ito, T.; Yoshida, Y.; Okauchi, T.; Obayashi, S.; Suhara, T.; Suzuki, K. *J. Med. Chem.* **2004**, *47*, 2228.
- Okubo, T.; Yoshikawa, R.; Chaki, S.; Okuyama, S.; Nakazato, A. *Bioorg. Med. Chem.* **2004**, *12*, 423.
- Zhang, M.-R.; Ogawa, M.; Furutsuka, T.; Yoshida, Y.; Suzuki, K. *J. Fluoro. Chem.* **2004**, *126*, 1879.
- Zhang, M.-R.; Tsuchiyama, A.; Haradahira, T.; Yoshida, Y.; Furutsuka, T.; Suzuki, K. *Appl. Radiat. Isot.* **2002**, *57*, 335.
- Melander, L.; Saunderson, W. H., Jr. *Reaction Rates of Isotopic Molecules*; John Wiley & Sons, 1980.
- Flowler, J. S.; Wang, G. J.; Logan, J.; Xie, S.; Volkow, N. D.; Schlyer, D. J.; Pappas, N.; Alexoff, D. L.; Patlak, C. J. *Nucl. Chem.* **1995**, *36*, 1255.
- Staley, J. K.; Van Dyck, C. H.; Tan, P.-Z.; Staley, J. K.; Tikriti, M.; Ramsby, Q.; Klump, H.; Ng, C.; Grag, P.; Soufer, R.; Baldwin, R. M.; Innis, R. B. *Nucl. Med. Biol.* **2001**, *28*, 271.
- Zhang, M.-R.; Haradahira, T.; Maeda, J.; Okauchi, T.; Kawabe, K.; Kida, T.; Obayashi, S.; Suzuki, K.; Suhara, T. *Nucl. Med. Biol.* **2002**, *29*, 469.
- Takei, M.; Kida, T.; Suzuki, K. *Appl. Radiat. Isot.* **2001**, *55*, 229.
- Chaki, S.; Funakoshi, T.; Yoshikawa, R.; Okuyama, S.; Okubo, T.; Nakazato, A.; Nagamine, M.; Tomisawa, K. *Eur. J. Pharmacol.* **1999**, *371*, 197.
- Okauchi, T.; Suhara, T.; Maeda, J.; Kawabe, K.; Obayashi, S.; Suzuki, K. *Synapse* **2001**, *41*, 87.
- Maeda, J.; Suhara, T.; Kawabe, K.; Okauchi, T.; Obayashi, S.; Hojo, J.; Suzuki, K. *Synapse* **2003**, *47*, 200.